Ion beam induced depth profile modification of H, D and He implanted in Be, C and Si

F. Schiettekatte [a], G.G. Ross [a,*], A. Chevarier [b], N. Chevarier [b], A. Plantier [b]

[a] *INRS- 'nergie et Mat'riaux, C.P.1020, 1650 Boulevard Lionel Boulet, Varennes, Qu'bec, Canada J3X1S2*
[b] *IPNL, Universit' Claude Bernard, F69622 Villeurbanne Cedex, France*

Abstract

A study has been made of modification induced by ion beam irradiation (350 keV He, 2.5 MeV He and 2.54 MeV N) on depth profiles of H, D and He implanted in beryllium, Highly Oriented Pyrolytic Graphite (HOPG) glassy carbon and silicon. Desorption rates have been measured as a function of depth. These rates can be related to models predicting activated (detrapped) atom profiles based on local molecular recombination. It is found that molecular recombination between *activated* atoms is a dominant mechanism for H and D implanted in carbon and beryllium with one important exception. In this case, of *high* concentration of H implanted in Be, stronger H and D trapping is observed in the vacancy profile. A higher desorption is also found to occur near the surface of crystalline samples. Finally, measured values of detrapping cross sections due to He and N beam bombardment are found to agree with a model which assumes that detrapping is induced by the primary recoils. © 1997 Elsevier Science B.V.

Keywords: Ion beam; Desorption; Depth profile; ERD; Implantation; Hydrogen; Deuterium; Helium; Beryllium; Carbon; Silicon; ^{15}N; Desorption rate; Primary recoil

1. Introduction

It is now well established that the properties of materials can be modified by the energy deposition due to swift ion irradiation [1]. One process is the induced desorption of some atoms or molecules contained in materials. But this effect also has consequences on the quantitative aspect of Ion Beam

Analysis [2], as well as on the plasma–wall interactions in Tokamak devices. Hence, many studies have been carried out on the desorption of fusion gases in materials [2–6], especially on the hydrogen isotopes in graphite.

However, it is difficult to determine how the incident ions interact with matter in order to detrap atoms. Some semi-empirical models were proposed to fit the total amount of remaining hydrogen as a function of beam fluence. They were generally based on simple or multiple exponential functions [6–9], as well as on the exponential inte-

*Corresponding author. Tel.: 514 929 8108; fax: 514 929 8102; e-mail: ross@inrs-ener.uquebec.ca.

gral [10]. Abel et al. [11] and Adel et al. [12] have proposed an equation that is based on a statistical distribution of ion impacts. Wampler and Myers [3] first proposed a physical model for carbon, including diffusion and retrapping to explain the desorption "slow down" at high fluence. All these models assume first order detrapping without in-bulk molecular recombination.

Scherzer et al. [4] added to Wampler's model a local molecular recombination term (second order) between activated (detrapped) atoms. According to anterior works, they assumed fast transport of these molecules to the surface. They also considered that the detrapping is induced by nuclear collisions between incident ions and trapped atoms. They calculated by means of TRIM [13] the corresponding detrapping rate for different beam energies. However, using a set of parameters obtained by fitting a data set at a given energy, the model gave only qualitative agreement for the other energies for which the data showed faster initial desorption rates. They suggested that another detrapping mechanism induced by the incident ion primary recoils could explain the discrepancy. In their opinion, this would however multiply at the same time the number of adjustable parameters.

Tsuchiya and Morita [5] have also studied hydrogen in graphite under MeV He irradiation. Their mass balance equations [14] assume local molecular recombination between trapped and activated atoms. By fitting an analytical solution of these equations to the desorption curves, they found the ion-induced detrapping cross section, σ_d, together with K/Σ_T, the ratio of the local molecular recombination constant divided by the retrapping constant. They showed that the experimental values and energy dependence of σ_d are in good agreement with theoretical predictions that assume detrapping induced by primary C recoils.

Nevertheless, if a few experiments have been performed on hydrogen profile modification by isotopic exchange at low (keV) energies in order to explain the desorption in this energy range (see for example Ref. [15]), only a few works studied in detail the depth profile modification of implanted materials. Such studies would confirm the process predicted by the models or reveal pos-

sible irregularities. So it becomes possible to highlight some phenomena such as stronger trapping in the implantation damage profile or the order of detrapping.

In this paper, we report the ion-induced depth profile modification of H, D and He implanted at low energies (keV) and at various concentrations in materials of interest for fusion (beryllium, graphitic and glassy carbon) and silicon. They were submitted to 350 keV ^{4}He, 2.5 MeV ^{4}He and 2.54 MeV ^{15}N beams, covering this way different ranges of energy deposition. The compatibility of the results with the models mentioned above will be discussed.

2. Desorption rate profile

Given the total concentration, $(,) = {}_t(,) + {}_s(,)$, where C_t and C_s are the concentrations of trapped and activated atoms, respectively, let the net detrapping rate be

$$\frac{d\,\tilde{(\;,\;)}}{d\;} = \sigma_d \phi\; {}_t(\;,\;) - \Sigma\; {}_s(\;,\;)[\,\tilde{}_0 - (\;,\;)],$$

(1)

where σ_d is the detrapping cross section of the incident particles, ϕ the beam flux, Σ the retrapping rate and $\tilde{}_0$ the trap density. On the one hand, for the high energy beam induced desorption, the model of Scherzer [4] can be expressed by the following rate equations:

$$\frac{d\;{}_s(\;,\;)}{d\;} = \frac{d\,\tilde{(\;,\;)}}{d\;} - {}_{ss}\;{}_s^2(\;,\;),$$

$$\frac{d\;{}_t(\;,\;)}{d\;} = -\frac{d\,\tilde{(\;,\;)}}{d\;},$$

(2)

where K_{ss} is the constant of molecular recombination between activated atoms. The solution of these equations with typical parameters shows that ${}_s^2(\;,\;) \propto (\;,\;)$.

On the other hand, the model of Morita [5] follows the rate equations:

$$\frac{d\;{}_s(\;,\;)}{d\;} = \frac{d\,\tilde{(\;,\;)}}{d\;} - {}_{st}\;{}_s(\;,\;)\;{}_t(\;,\;),$$

$$\frac{d\;{}_t(\;,\;)}{d\;} = -\frac{d\,\tilde{(\;,\;)}}{d\;} - {}_{st}\;{}_s(\;,\;)\;{}_t(\;,\;),$$

(3)

where K_{st} is the constant of molecular recombination between activated and trapped atoms. By solving Eq. (3) using typical parameters, we find that $_s(\ ,\ ) \propto (\ ,\ )$. In both cases, $_s(\ ,\ ) \ll _t(\ ,\ ) \lesssim \ _.$

Assuming a constant beam flux ϕ (with the beam fluence $\varphi = \phi$), the *desorption* rate (not to be confused with the *detrapping* rate) can be defined as

$$(\ ,\varphi) = -\frac{1}{(\ ,\varphi)}\frac{d\ (\ ,\varphi)}{d\varphi}$$

$$= -\frac{1}{(\ ,\varphi)}\left(\frac{d\ _s(\ ,\varphi)}{d\varphi} + \frac{d\ _t(\ ,\varphi)}{d\varphi}\right). \quad (4)$$

$(\ ,\varphi)$ gives the ratio of desorption at depth x relative to the concentration of the depth profile $(\ ,\varphi)$. It appears that for Scherzer's model

$$(\ ,\varphi) = \frac{ss\ _s^2(\ ,\varphi)}{(\ ,\varphi)}$$

$\sim$ constant with depth,   (5)

while for Morita's model

$$(\ ,\varphi) = \frac{2\ _{st}\ _s(\ ,\varphi)\ _t(\ ,\varphi)}{(\ ,\varphi)} \sim (\ ,\varphi). \quad (6)$$

The desorption rate $(\ ,\varphi)$ can be found experimentally using two successive profiles separated by a small fluence $\Delta\varphi$

$$(\ ,\varphi) \approx \frac{(\ ,\varphi - \Delta\varphi) - (\ ,\varphi)}{(\ ,\varphi)\Delta\varphi}. \quad (7)$$

In this paper, $Y(x)$ has been calculated for many depth profiles. The raw data for $Y(x)$ are represented with arbitrary units by $\bigcirc$ symbols. The statistical error on $Y(x)$ is equal to the data point dispersion. Because the starting depth profiles are still resolution-broadened, the measured $Y(x)$ is found to be smoothed relatively to the actual curve. This kind of curve will be helpful in determining the uniformity (or non-uniformity) of the detrapping process, to validate models and to find if diffusion plays a role in desorption. Even if these models were developed for graphite, they will be used to discuss the desorption of hydrogen in beryllium for which no specific physical model is available.

3. Experimental

To conduct this study, good depth resolution is necessary to get relevant depth profiles. Like most of the papers mentioned above, ERD [16] was used because it gives quantitative depth profiles and the ion-induced desorption is intrinsic to the technique. Moreover, the use of an $E \times B$ filter [17] (instead of an absorber foil) only limits the surface resolution to the detector resolution. Together with a beam close to the stopping power maximum, the depth resolution is optimal and sufficient for relevant observation of the depth profile modification. The 350 keV ^{4}He irradiation was also monitored by means of Multi-Channel Scaling (MCS) which allows one to follow more precisely the evolution of the total amount of implanted atoms during irradiation.

A description of the experimental setups used and the resolution calculation can be found in [18]. Briefly, the 350 keV ^{4}He analyses, were done with an incident angle of 25° relative to the sample surface and a scattering angle of 45°. The solid angle was 2.06×10^{-5} str. The 2.5 MeV ^{4}He and 2.54 MeV ^{15}N analyses were performed with an incident angle of 15° relative to the sample surface and a scattering angle of 30°. The solid angle was 6.6×10^{-5} str. Solid angles were chosen to be small in order to minimize the spatial spread of the scattered particles so that they can be separated properly inside the $E \times B$ filter. Obviously, this worsens the sensitivity as well. The depth resolution (σ) will be plotted as a horizontal error bar on some graphs. All the depth profiles (and scaling data) shown in this paper are accumulated depth profiles, i.e. they contain all the detected particles from the start of the measurement to the corresponding fluence. The statistical error on the first point of each scaling data set is always $\leqslant 10\%$.

The materials used are available commercially. The beryllium samples (Be, Beryllium Window) are polycrystalline (grain size ≈ 1 μm) with a 99.4% purity. The Highly Oriented Pyrolytic Graphite (HOPG, Union Carbide) contains 6% hydrogen as its main impurity. It has been implanted along the *a*-orientation. The glassy carbon (v-C, Carbone Lorraine) is amorphous and contains no measurable quantity of hydrogen. The sil-

icon (Si) comes from an n-Si $\langle 1\,0\,0 \rangle$ wafer and is of the purity standard set by the semiconductor industry. The Be, HOPG and v-C samples were polished with a 3 μm diamond suspension followed by a 0.04 μm alumina finish. The Si samples were not polished. Nearly 100 samples were implanted with different energies and doses. The details will be given for each ion–material combination.

The ERD energy spectra were converted to depth profiles by means of Alegria, a Windows 95 freeware available from the authors. Alegria is described in [19]. The profiles are still resolution broadened.

4. Results and discussion

The depth profile modification is somewhat different from one material to the next. The mechanisms involved in the desorption process can be very different. Therefore, the results are presented separately for each material. The H, D and He profile modifications are shown for each of these. Helium profiles were only measured by 2.54 MeV ^{15}N irradiation. It is important to note that at these energies the sputtering yields induced by He and N at an angle of 15° relative to the surface are below 0.01 and 0.1, respectively. So this induces a negligible depth shift to the profiles.

4.1. Beryllium

4.1.1. H in Be

Be samples were implanted with hydrogen at energies of 0.8 and 1.5 keV and fluences ranging from 1.9×10^{16} to 2.6×10^{17} H/cm^2 that correspond to peak concentrations between 0.05 and 0.62 H/Be. The H saturation concentration is near 0.3 H/Be, so some samples were oversaturated. However, the implantation damage continues to increase for these samples.

Under 2.5 MeV and 350 keV He irradiations, the hydrogen profiles are relatively stable in samples where the peak concentration does not exceed 0.12 H/Be. H desorption and depth profile modification begin to be observed above this ratio, and the desorption rate increases with the concentration. Results presented in Fig. 1 are those for the
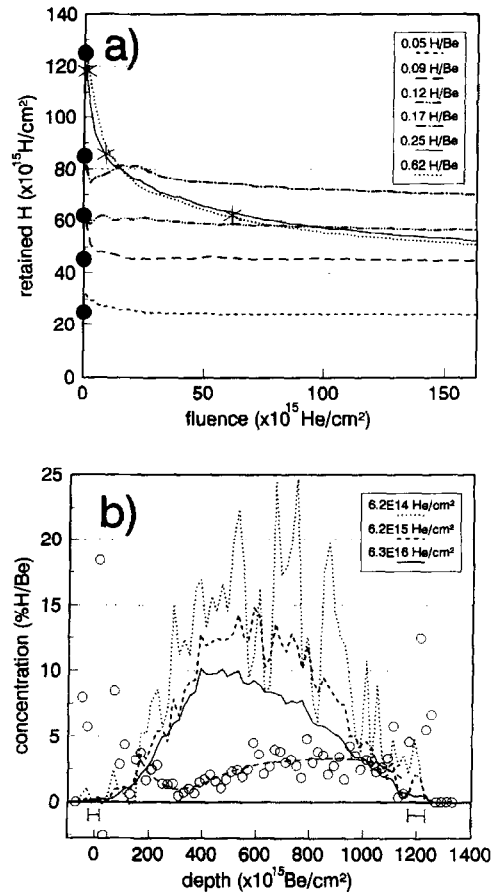

Fig. 1. 1.6 keV H implanted in Be after 350 keV ^{4}He irradiation (a) MCS data (symbols ● represent the implanted concentration while symbols * represent the H quantity found in (b). (b) H depth profile modification for the 0.62 H/Be sample. The desorption rate as a function of depth (— ○ —) after a fluence of 6.3×10^{16} He/cm^2 also appears.

1.5 keV implantations irradiated by the 350 keV ^{4}He beam. It appears in (a) that at high He fluences, the samples implanted at 0.25 and 0.62 H/Be have a lower final retained quantity of H than the sample implanted at 0.17 H/Be, and this H quantity gets even smaller than in the 0.12 H/Be sample. This is compatible with observations following laser induced desorption [20] and thermal desorption [21] where a significant decrease of the detrapping energy was seen above a similar H concentration (0.15 H/Be) for all atoms. This also corresponds to the threshold where blistering starts to appear after implantation. Laser induced

desorption indicated also that the desorption process is no longer limited by diffusion for those concentrations.

Fig. 1(b) shows the H depth profile modification in the 0.62 H/Be sample at He fluences corresponding to the symbols * in Fig. 1(a). The desorption rate $Y(x)$ is calculated for the highest fluence profile (6.3×10^{16} He/cm^2). As it will be seen for ^{15}N irradiation, the minimum $Y(x)$ under the surface corresponds to the implantation damage profile (vacancies). If a fraction of the H atoms at this depth are trapped in vacancies instead of in interstitial sites, they are certainly bound with a higher energy. Besides, this zone could also act as a drain where the diffusing atoms or molecules from larger depths are retrapped. No retrapping is observed in depth (deeper than the profile), so no diffusion occurs in that direction.

Under ^{15}N irradiation, the hydrogen desorbs rapidly in all samples. Moreover, above the 0.15

H/Be threshold, the desorption process is much larger. Fig. 2(a) shows the evolution of the total quantity of H implanted at 0.8 keV and fluences between 1.9×10^{16} and 1.5×10^{17} H/cm^2 that correspond to peak concentrations ranging from 0.05 to 0.40 H/Be. In this graph, the solid symbols represent the implanted dose of H, also confirmed by 2.5 MeV ^{4}He beam measurement. However, for the sample implanted to 0.40 H/Be, the solid symbol corresponds to the *retained* H quantity measured by the 2.5 MeV ^{4}He beam. It is seen that the H concentration in the 0.05 H/Be sample rapidly reaches a plateau (7.5×10^{15} H/cm^2), while in the 0.15 H/Be sample H concentration still decreases at higher N fluences. It is impressive to see that the 0.25 and 0.40 H/Be samples have lost nearly 50% of their hydrogen after irradiations of only 6×10^{13} N/cm^2. The final H quantity of both samples are even much lower than that in the 0.15 H/Be sample. For the 0.25 and 0.40 H/Be samples,
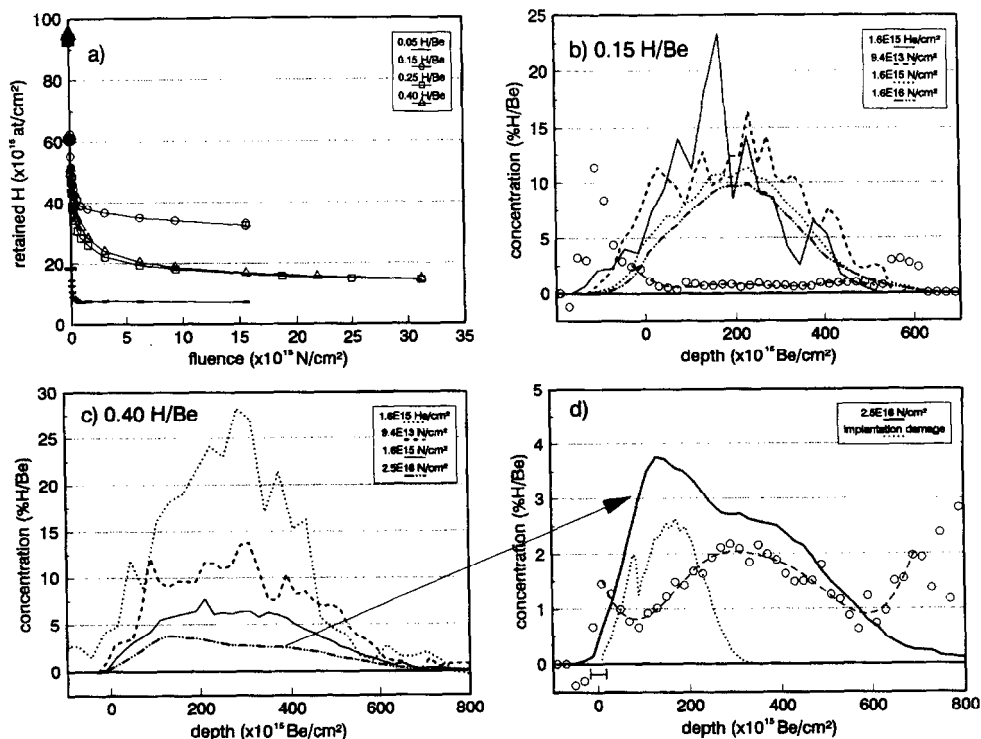

Fig. 2. 0.8 keV H implanted in Be after 2.54 MeV ^{15}N irradiation. (a) Evolution of H quantity. (b) H depth profile evolution in the 0.15 H/Be sample. (c) H depth profile evolution in the 0.40 H/Be sample. The last fluence profile appears also in (d) together with the vacancy profile. In both (b) and (d), symbols $- \ominus -$ are the desorption rates.

both curves superimpose (similar initial retained H concentration) so it seems that there is no effect due to the increase of implantation damage.

Fig. 2(b) shows the H depth profile evolution in the 0.15 H/Be sample. It is seen that at high ^{15}N fluences, the desorption rate $Y(x)$ is almost constant on all depth ranges except for the rise near the surface. This effect was not observed after 350 keV [4]He beam irradiation because of the relative stability of H.

Above this concentration (0.15 H/Be), we observe the same type of H profile modification as seen under 350 keV [4]He irradiation. The H depth profile modification in the 0.40 H/Be sample is shown in Fig. 2(c). The highest fluence profile is also plotted in Fig. 2(d) together with the vacancy profile (calculated by means of TRIM-95 [13]). Once more, a minimum in the desorption rate is seen just under the surface. Moreover, the vacancy profile exactly matches with the peak in H depth profile. At this time, a maximum arises in the desorption rate profile. No in-depth diffusion is observed.

Thus, the beam induced detrapping of hydrogen implanted in Be follows two different regimes depending on the initial H concentration. At H peak concentrations $\leqslant 0.12$ H/Be, H is more firmly bound. The desorption rate profile could be compatible with Scherzer's model. Above this critical concentration, the desorption rate profile starts to follow the shape of the profile except in the damaged zone where the trapped particles are bound with higher energy. This effect was not observed under the critical H concentration. In that regime, the desorption rate complies with Morita's model. Because no in-depth diffusion is observed, the unimplanted, unirradiated Be seems to act as a diffusion barrier.

4.1.2. D in Be

1.6 keV D with fluences ranging from 1.0×10^{16} to 2.5×10^{17} D/cm^2 was implanted in Be and analyzed by means of 350 keV [4]He and 2.54 MeV ^{15}N beams. As seen in Fig. 3(a), although there is no D desorption under He irradiation in samples with D peak concentrations $\leqslant 0.15$ D/Be, the desorption rate of the sample implanted to 0.30 D/Be is slower than for H. In Fig. 3(b), the D profile evolution of
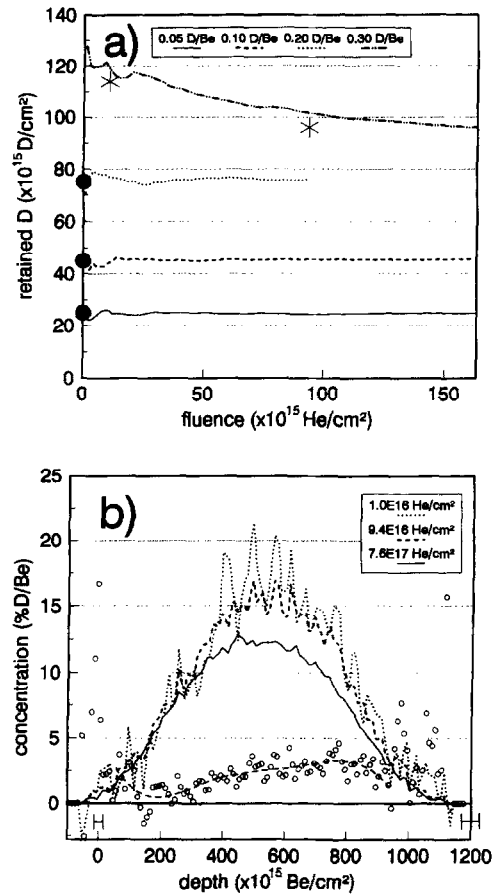

Fig. 3. 1.6 keV D implanted in Be after 350 keV [4]He irradiation (a) MCS data (symbols * represent the H quantity found in (b). (b) D depth profile modification for the 0.30 D/Be sample. The desorption rate (– ⊖ –) after a fluence of $(9.4 \times 10^{16}$ He/cm^2) also appears.

the 0.30 D/Be sample following He irradiation shows almost the same shape of desorption rate observed for the H (Fig. 1(b)). Thus, even if the D desorbs more slowly, the same transition is observed.

4.1.3. He in Be

Helium was implanted in Be at energies of 0.8, 1.5, 5 and 10 keV with fluences ranging from 4.7×10^{15} to 1.0×10^{17} He/cm^2. Helium was profiled by a 2.54 MeV ^{15}N beam. In spite of the high energy deposition, only little He desorption is observed (<5%). This is consistent with the observa-

tions of Jung [22] who found only little thermal desorption of the implanted helium even at a temperature close to the melting point. Obviously, helium atoms are detrapped in a first order process. Two possibilities come to light to account for this: (1) the trapped helium is bound with an energy high enough to prevent any detrapping, (2) its diffusion coefficient is so low that it is retrapped before it has time to move in the lattice. A heavier beam (with higher energy deposition) could be used in order to determine if He atoms are finally detrapped and desorbed or if the diffusion process still limits its desorption.

4.2. Highly oriented pyrolytic graphite

4.2.1. H in HOPG

HOPG was H implanted with energies of 0.8 and 1.5 keV and fluences ranging from 1.0×10^{16} to 1.3×10^{17} H/cm^2 that correspond to peak concentrations ranging from 0.05 to 0.35 H/C. Thus, the saturation of 0.4 H/C was not reached or exceeded. It is worth mentioning that HOPG already has a 0.06 H/C background that also desorbs.

In these experiments, He beam induced desorption is observed for all concentrations as shown in Fig. 4(a) for the 1.5 keV H implantations. In these measurements, the H background represents 5×10^{16} H/cm^2 of the initial concentration. It is seen in Fig. 4(a) that from one He fluence to another, there is a similar difference in the retained quantity of H except for the 0.30 H/C sample at low beam fluence. This could be explained if one assumes that: (1) the 6% H background is responsible for the most part for the initial decrease in the 0.05, 0.10 and 0.25 H/C samples so that very similar absolute H quantities were released from these samples during the first 3×10^{16} He/cm^2 irradiation; (2) the H background was desorbed from the 0.30 H/C sample during the implantation because it was implanted close to saturation, so no such H background desorption is observed at low He beam fluence. Thus, the implanted H desorbs more slowly than the H background. Besides, at high fluence, the implanted H desorption increases gradually with concentration, but the total H quantity in a sample never falls below
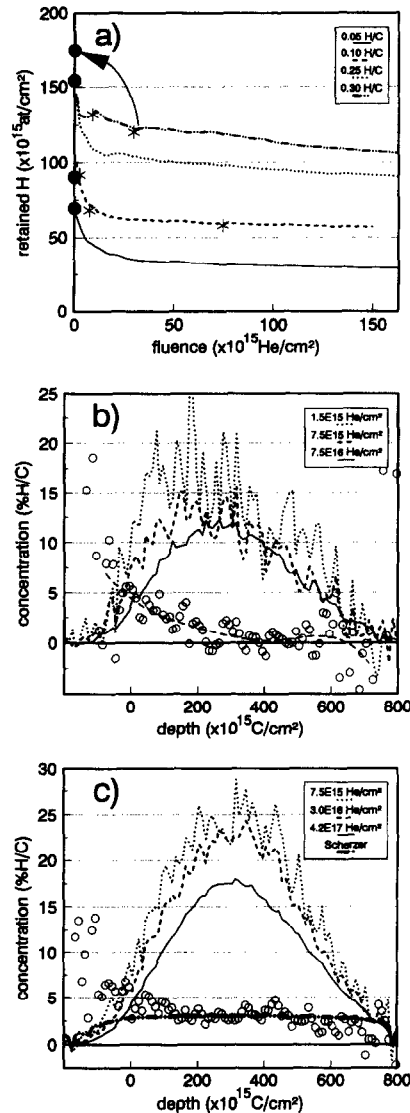

Fig. 4. 1.5 keV H implanted in HOPG after 350 keV ^{4}He irradiation. (a) MCS data. Symbols ● represent the implanted concentration including H background while symbols * are the H quantity found in (b) and (c). (b) H depth profile modification for the 0.10 H/C sample. The desorption rates data (− ⊝ −) after a fluence of 7.5×10^{16} He/cm^2 is also shown. (c) H depth profile modification for the 0.30 H/C samples. Also appearing are the desorption rate data (○) after a fluence of 3.0×10^{16} He/cm^2 and the desorption rates calculated according to Scherzer's model (− · −).

the H quantity of another sample implanted at lower concentration, as seen in beryllium above 0.15 H/Be.

Fig. 4 also shows H depth profile modification for low (b) and high (c) H/C concentrations. H desorption occurs preferentially near the surface. In Fig. 4(b), the H desorption rate from the 0.10 H/C sample, following a high 350 keV ^{4}He fluence, decreases continuously from the surface until a depth of 4×10^{17} C/cm^2. This decrease will be called "surface ramp". In Fig. 4(c) the same feature is observed in the 0.30 H/C sample. However, the surface ramp is overcome by a constant desorption rate. The value of this constant desorption rate augments with the H concentration and complies with Scherzer's model (also plotted in Fig. 4(c)). The surface ramp points out that a diffusion process probably occurs so that the hydrogen closer to the surface is more easily desorbed. This process is not influenced by the sample H concentration. An identical surface ramp is observed for the lower energy implantation (0.8 keV) but it covers the entire range of implantation. Hence, the surface ramp seems to have a constant maximum depth. Similar diffusion and retrapping process could be responsible for the $Y(x)$ decrease at the end of both profiles ($\sim 7 \times 10^{17}$ C/cm^2).

As expected, Fig. 5 shows that under ^{15}N bombardment H desorption is much faster. Only the 0.8 keV H implanted samples were depth profiled. Fig. 5(a) shows the evolution of the total H quantity as a function of N fluence. Solid symbols represent the H dose as measured by means of a low fluence 2.5 MeV ^{4}He beam. Once again, a part of the total dose ($\sim 6 \times 10^{16}$ H/cm^2) comes from the 0.06 H/C background that also desorbs. As seen for H in Be, very high initial H desorption occurs below 6×10^{13} N/cm^2 for the higher H concentration samples. It is seen that $\sim$60% of the H is desorbed in the first 6×10^{13} N/cm^2 irradiation. However, at a given N fluence, the total H quantity in a sample is always higher than the H quantity of another sample implanted at lower concentration, as observed under 350 keV ^{4}He irradiation.

Fig. 5(b) shows the H depth profile modification in the 0.35 H/C sample together with the desorption rate (Fig. 5(c)). This desorption rate induced by a high N fluence features a surface ramp that extends far in depth to 10^{18} C/cm^2. Thus, it seems that the beam species influences the maximum depth of the surface ramp. Also,
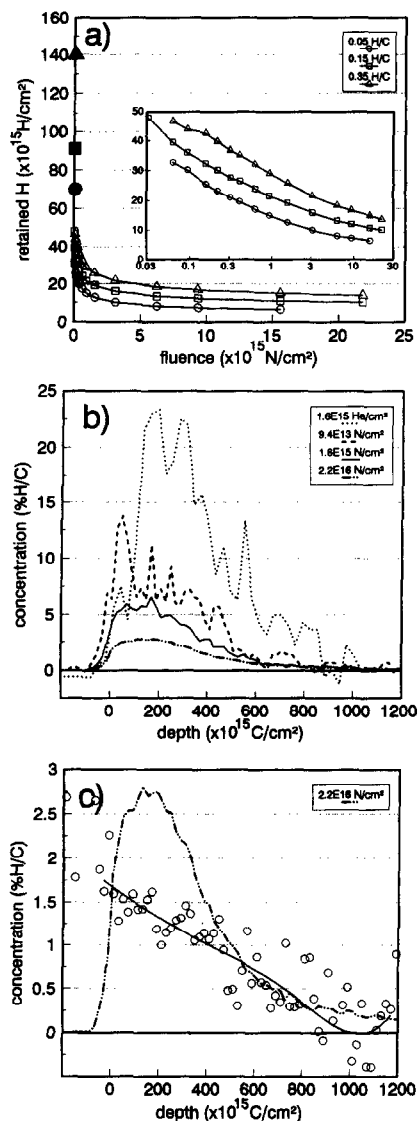

Fig. 5. 0.8 keV H implanted in HOPG after 2.54 MeV ^{15}N irradiation. (a) Evolution of H quantity; the inset is the same graph plotted with a logarithmic fluence scale. (b) H depth profile evolution in the 0.35 H/C sample. (c) Desorption rate data (– ⊖ –) for the highest N fluence profile.

no constant detrapping rate is observed as seen for a similar implanted concentration after 350 keV ^{4}He irradiation (Fig. 4(c)). However, the desorption rate was calculated after a high fluence N bombardment, so the H concentration of the profiles is very low ($\sim$2%). Hence, this case is more similar to Fig. 4(b). In both cases, the net detrap-

ping rate (Eq. (1)) is low because the number of available traps is high. The desorption of activated atoms vanishes accordingly, while the process corresponding to the surface ramp is still active.

To sum up, the mechanism for H desorption in HOPG can be modeled in part by Scherzer's equations. However, this model does not explain the surface ramp for which diffusion to the surface is more likely to be the driving force. Contrary to H in Be, no preferential trapping is observed in the implantation damage profile (which is low for graphite). In the H concentration range covered in our experiment, the desorption simply increases with concentration without any particular irregularity due to H concentration. At low concentrations (H/C < 0.15), the desorption process is somewhat faster than for H in Be (H/Be < 0.15). The H desorption from the 0.06 H/C background is faster than the desorption of the implanted H, but this is not sufficient to account for the very high desorption at very low N fluence, at least in the HOPG samples implanted to high H concentrations.

4.2.2. D in HOPG

Because the ERD sensitivity is much lower for deuterium (cross section is lower), the D depth profile modification is more difficult to analyze. However, if moderated H desorption was observed under 350 keV ^{4}He irradiation, only very low desorption occurs for D. D desorption induced by 2.54 MeV ^{15}N irradiation is also lower than for H. D implanted in a HOPG sample to a low concentration was profiled by means of a ^{15}N beam. 82% of the D was retained after a fluence of 1.5×10^{15} N/cm^2 while less than 60% of the implanted H was retained in the 0.05 H/C sample (Fig. 5(a)). Once more, an important isotopic effect is observed in the trapping energy and/or detrapping probability. However, the desorption process is similar for H and D. The desorption rate is constant all over the depth profile, in agreement with Scherzer's model. As observed for H, preferential D desorption occurs near the surface.

4.2.3. He in HOPG

Helium is not retained in HOPG when implanted at low energy. Only He implanted at 10 keV

was retained (25%). Helium is necessarily detrapped in a first order process. However, the evolution of the total He quantity following N irradiation does not correspond to an exponential. Fig. 6 shows the He depth profile modification after 2.54 MeV ^{15}N irradiation. As observed for H, preferential desorption occurs closer to the surface. In bulk, the desorption rate decreases with depth as seen for H in HOPG. However, the desorption rate becomes very high in the first 2×10^{17} C/cm^2 depth. Hence, diffusion becomes more important close to the surface. This could be explained by the crystallinity of the HOPG provided that He is trapped in the crystal defects. Therefore, desorption of He in HOPG follows a desorption mechanism similar to H's at low concentration.

4.3. Hydrogen in glassy carbon (v-C)

Contrary to HOPG which is highly oriented polycrystalline structure, v-C has a uniform amorphous structure. It was observed that H implanted to a peak concentration of 0.10 H/C is stable under 350 keV ^{4}He irradiation. However, the 0.40 H/C sample undergoes a large decrease in its H content (50% after 4.2×10^{16} He/cm^2 irradiation). Fig. 7 shows the H profile modification for this sample. At high He fluence, it appears that the desorption
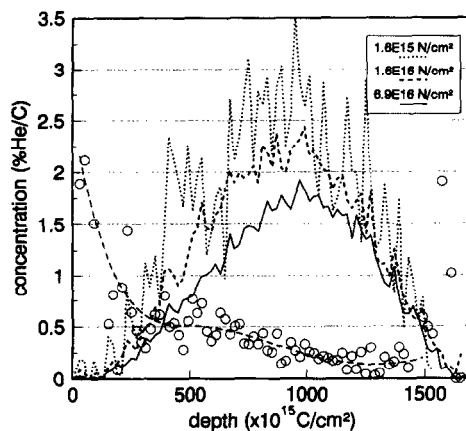

Fig. 6. Depth profile modification of 10 keV He implanted in HOPG to fluence of 1×10^{17} He/cm^2 after N irradiation. The desorption rate data (– ⊝ –) also appears.
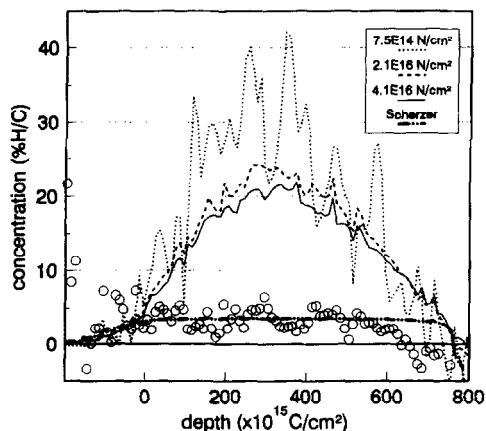
Fig. 7. Depth profile modification of 1.5 keV H implanted in v-C to a fluence of 1.7×10^{17} H/cm² after N irradiation. Also appearing are the desorption rate data (○) and desorption rates calculated according to Scherzer's model (— · · —).

rate is uniform all over the depth profile except for a decrease (and some retrapping) deeper than 6×10^{17} C/cm². Except for that feature, which could be due to diffusion, the desorption process is compatible with Scherzer's model. The H detrapping rate profile does not show a surface ramp as observed in the HOPG. This could indicate that the surface ramp was due to enhanced diffusion close to the surface because of the local crystallinity of the HOPG near the surface.

4.4. H and He in silicon

A few Si samples were implanted with 0.8 keV H and 1.6 keV He at normal incidence (with a possibility of low energy channelling [23]) to fluences ranging from 1.7×10^{16} to 7.5×10^{16} H/cm² and from 2.4×10^{15} to 1.0×10^{16} He/cm², respectively. As observed in previous works [2], no H desorption occurs under 350 keV ⁴He irradiation. H and He depth profiles were also obtained by means of a 2.54 MeV ¹⁵N beam. Fig. 8(a) shows the evolution of the total H and He quantity after different N fluences. Solid symbols represent the implanted doses. The desorption rates are moderated or low, except for the 0.15 H/Si sample. Its depth profile is plotted in Fig. 8(b) for different N fluences. An important surface peak is present
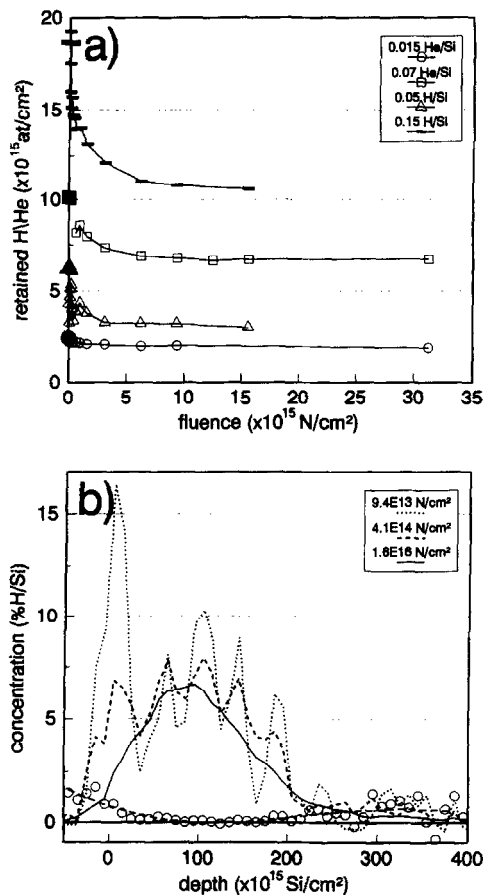

Fig. 8. 0.8 keV H and 1.6 keV He implanted in Si after 2.54 MeV ¹⁵N irradiation. (a) Evolution of the total H or He quantity. (b) H depth profile evolution in the 0.15 H/Si sample together with the desorption rate (− ⊖ −).

at low N fluence and vanishes rapidly. This could be due to surface water vapor adsorption but no such peak was observed with 2.5 MeV ⁴He beam. Also, during the experiment a LN₂ cold trap was used. This usually eliminates water vapor contamination. Another possible explanation is that the H desorption occurs by atomic H diffusion followed by molecular recombination on the silicon surface. H has a high surface binding energy on Si relative to Be and C. H atoms were still adsorbed on Si surface during initial (high rate) detrapping. Because H in Si is stable under He irradiation, it would not have been observed.

5. Detrapping cross section

Figs. 4(c) and 7 show that the model of Scherzer [4] complies with the H desorption rate profile observed in carbon. However, the authors assumed that H detrapping occurs through nuclear collisions between incident ions and trapped atoms. According to the authors themselves and as mentioned in the introduction, this detrapping mechanism is not sufficient to explain the early desorption rate. Tsuchiya and Morita have considered the hydrogen detrapping induced by primary recoils and have developed a theoretical expression for the detrapping cross section σ_d [5]. This equation predicts a lower desorption rate for D compared to H and states that,

$$\sigma_d \propto \frac{2}{\text{beam}} \quad \text{beam} \cdot \tag{8}$$

They implanted H to saturation in graphite and measured σ_d after He irradiation of energies ranging from 800 keV to 1.9 MeV. They found good agreement between their experimental and theoretical values. For saturated samples, the detrapping cross section can be found from the early desorption rate (at very low beam fluence), because the retrapping process (right-hand side of Eq. (1)) is small in saturation conditions. For H implanted to saturation in HOPG, our σ_d values are also in relatively good agreement with the Tsuchiya and Morita equation. We found $\sigma_d = 2.5 \times 10^{-17}$ with the 2.5 MeV ^{4}He beam and $\sigma_d = 9.2 \times 10^{-16}$ with the 2.54 MeV ^{15}N beam. The ratio of 37 between these two values is in fairly good agreement with the ratio of 46 predicted by Eq. (8). Moreover, we found that the D detrapping rates were lower than the H ones, as predicted by the Tsuchiya and Morita equation.

6. Conclusion

A study of the depth profile modification of H, D and He implanted in materials under high energy ion beam irradiation has been presented. The good depth resolution of the ERD-$E \times B$ technique has allowed to measure for the first time the desorption rates of H, D and He as a function of depth, which can be connected to the activated (detrapped) atom profiles according to Scherzer's and Morita's physical models. Table 1 gives a summary of the results. The effect of the different beam species and energies on the total amount can be assessed. It is clearly seen that the decrease of the implant concentration is relatively higher for samples implanted to high concentrations compared to those implanted to low concentration (except for the HOPG implanted with H). In the HOPG samples, the effect is equivalent or even stronger for low H concentrations. This is due to the H background that desorbs more rapidly than the implanted H. Because it contributes to a larger proportion to the total amount in the low concentration samples, the H desorption appears to be stronger. However, if the effect of the H background is subtracted, the H desorption is found to be higher for HOPG samples implanted to high H concentration. Table 1 also shows that an isotopic effect is observed in all samples when H and D desorption is compared. D desorption is always much lower.

The desorption rates of H and D in carbon at high beam fluences validate Scherzer's model which assumes recombination between activated atoms. It does not explain the enhanced desorption surface ramp observed in HOPG. This ramp, which was not seen in glassy carbon, was probably due to HOPG's crystallinity. The desorption of H implanted at low concentration in Be (<0.12 H/Be) also complies with Scherzer's model. However, at high H concentrations, the desorption rate is minimal in the vacancy profile region while in deeper regions it follows the profile shape. Therefore, it complies with Morita's model in the deeper region. The transition in the H desorption level seen above 0.12 H/Be was also observed by laser induced desorption [20] and thermal desorption [21]. It corresponds to the threshold where blistering starts to be observed after implantation.

The detrapping cross sections of the He and N beams are in agreement with the Tsuchiya and Morita equation which assumes that the desorption is induced by the primary recoils. The N beam was used to see the effect of a higher energy deposition on depth profile modification. The high H desorption rates measured suggest caution when using some Nuclear Resonance Reaction Analysis

Table 1
Summary table: Percentage of implant retained after low and high beam fluences

Mater.	Beam (keV)	Implant	Retained after 10^{14} at/cm^2 (lower/higher concentration)	Retained after 1.5×10^{16} at/cm^2 (lower/higer concentration)	Model
Be	^{4}He (350)	H	100% / 100%	>90% / 60%	?/M
		D	100% / 100%	100% / 88%	?/M
	^{4}He (2500)	H	n.a./ 100%	n.a./ 74%	n.a./S
	^{15}N (2540)	H	100% / 55%	50% / 17%	S/M
		^{4}He	n.a./ 100%	n.a./ >90%	
v-C	^{4}He (350)	H	100% / 100%	>90% / 76%	?/S
HOPG		H	100% / 100%	67% / 76%	S*/S
		D	100% / 100%	100% / >90%	?
	^{4}He (2500)	H	100% / 100%	57% / 70%	S/S
	^{15}N (2540)	H	54% / 34%	8% / 10%	S*/S*
		D	100% / n.a.	82% /n.a.	S/n.a.
		^{4}He	25% after implantation	80% (of initial 25%)	
Si	^{4}He (350)	H	100% / 100%	100% / 100%	?
		D	100% / 100%	100% / 100%	?
	^{15}N (2540)	H	100% / 100%	48% / 57%	
		^{4}He	100% / 100%	86% / 68%	

?: Not enough desorption to calculate relevant desorption rate profile.
*: No constant desorption rate was actually observed (Scherzer's model) due to the low concentration even if related results support it.
Note: The values for the lowest and highest implanted concentration are shown (generally around 5 at% and ∼35 at%, respectively).
The relevant physical model also appears (S = Scherzer, M = Morita).

(NRRA) for the high resolution profiling of hydrogen (e.g. p(^{15}N,α)^{12}C at 6.385 MeV [24]).

Acknowledgements

References

[1] J. Davenas, A. Dunlop, F. Rullier-Albenque, C. Jaouen, C. Templier, Materials under irradiation, Solid State Phenomena, vols. 30,31, Trans. Tech., 1993.
[2] G.G. Ross, I. Richard, Nucl. Instr. and Meth. B 64 (1992) 603.
[3] W.R. Wampler, S.M. Myers, J. Nucl. Mater. 111,112 (1982) 616.
[4] B.M.U. Scherzer, W. Wielunski, W. Möller, A. Turos, J. Roth, Nucl. Instr. and Meth. B 33 (1988) 714.
[5] B. Tsuchiya, K. Morita, J. Nucl. Sci. Tech. 31 (1994) 1301.
[6] J. Roth, B.M.U. Scherzer, R.S. Blewer, D.K. Brice, S.T. Picraux, W.R. Wampler, J. Nucl. Mater. 93,94 (1980) 601.
[7] J.P. Bugeat, E. Liegeon, Nucl. Instr. and Meth. 159 (1979) 117.
[8] B.M.U. Scherzer, R.S. Blewer, R. Behrisch, R. Schulz, J. Roth, J. Borders, R. Langley, J. Nucl. Mater. 85,86 (1979) 1025.
[9] H. Baumann, T. Rupp, K. Bethge, P. Koild, C. Wild, European Mater. Res. Soc. Conf. Proc. 17 (1987) 343.
[10] S. Turgeon, R.W. Paynter, Nucl. Instr. and Meth. B 118 (1996) 322.
[11] F. Abel, V. Quillet, M. Schott, Nucl. Instr. and Meth. B 105 (1995) 86.
[12] M.E. Adel, O. Amir, R. Kalish, L.C. Feldman, J. Appl. Phys. 66 (1989) 3248.
[13] J.F. Ziegler, J.P. Biersack, The Stopping and Range of Ions in Solids, Pergamon Press, New York, 1985.
[14] K. Morita, Y. Hasebe, J. Nucl. Mater. 176,177 (1990) 213.
[15] S. Nagata, S. Yamaguchi, H. Bergsåker, B. Emmoth, Nucl. Instr. and Meth. B 33 (1988) 739.
[16] J. L'Écuyer et al., J. Appl. Phys. 47 (1976) 381.
[17] G.G. Ross, L. Leblanc, Nucl. Instr. and Meth. B 83 (1993) 15.
[18] F. Schiettekatte, A. Chevarier, N. Chevarier, A. Plantier, G.G. Ross, Nucl. Instr. and Meth. B 118 (1996) 307.
[19] F. Schiettekatte, G.G. Ross, Proceedings of the 14th International Conference on the Application of Acceler-

ators in Research and Industry, CP392 AIP Press, New York, 1997, 711.

[20] F. Schiettekatte, D. Kéroack, G.G. Ross, B. Terreault, Nucl. Instr. and Meth. B 90 (1994) 401.

[21] W.R. Wampler, J. Nucl. Mater. 122 (1984) 1598.

[22] P. Jung, J. Nucl. Mater. 202 (1993) 210.

[23] G. Bourques, B. Terreault, Nucl. Inst. Meth. B 115 (1996) 468.

[24] W.A. Landford, H.P. Trautvetter, J.F. Ziegler, J. Keller, Appl. Phys. Lett. 28 (1976) 566.